ELSEVIER

International Journal of Mass Spectrometry 178 (1998) 187–204

International Journal of Mass Spectrometry

Sample charge compensation via self-charge-stabilizing ion optics

David A. Dahl*, Anthony D. Appelhans

Idaho National Engineering and Environmental Laboratory, Idaho Falls, ID 83415, USA

Received 23 March 1998; accepted 30 July 1998

Abstract

A self-charge-stabilizing ion optics method to control electrostatic sample charging of insulators bombarded with energetic particles has been developed and evaluated. In this method, ion optical elements form a simple self-controlling electrostatic field servo loop that automatically limits sample charging. The method has been applied successfully with insulating samples for secondary ion mass spectrometry in both quadrupole and ion trap based instruments. Self-charge-stabilizing ion optics appears to be a direct way to prevent or control sample charging in those circumstances where the approach is applicable. (Int J Mass Spectrom 178 (1998) 187–204) © 1998 Elsevier Science B.V.

Keywords: Ion optics; Sample charging; Secondary ion mass spectrometry; Ion trap

1. Introduction

Analytical techniques like Secondary Ion Mass Spectrometry (SIMS) make measurements via the use of charged particles that are absorbed by and/or emitted from samples. If the net flux of charge transported to and from the sample is not zero, samples that are electrical insulators can quickly charge to hundreds of volts. This creates serious problems because uncontrolled electrostatic charging of samples can prevent downstream ion optics components from focusing or detecting the secondary ions properly.

The most commonly used sample charge compensation method for SIMS involves flooding the sample with a low energy electron beam [1]. Since most samples charge positively, an appropriately controlled influx of low energy electrons can successfully compensate for charging. Unfortunately, electron bombardment of the sample can also damage the surface, complicating the interpretation of the results [2]. Charge compensation by electron flooding is even more challenging when negatively charged secondary ions are being analyzed, because the flood electrons must be directed uphill (electrostatically) toward the sample against the prevailing secondary ion extraction field.

Another charge compensation method called pulsed extraction has been developed by our group [3]. A high energy neutral (uncharged) or negatively charged primary beam is used to impact the sample, while an alternating polarity extraction field is applied near the sample. This results in periods when positive or negative secondary ions are being extracted from the sample while ions of the opposite polarity are

* Corrresponding author.

PII S1387-3806(98)14120-9

being repelled back toward the sample. The frequency of the pulsed extraction potential is normally around 20 Hz. Charge compensation is accomplished by varying the relative duration of the positive and negative ion extraction periods to keep the sample's potential oscillating within a desired range.

Pulsed extraction was expected to behave much like charging a capacitor. If no net current (e.g. net charge flux) enters or leaves the capacitor its *average* potential will remain constant. However, if a small net current flows (e.g. the pulse ratio is slightly miss-adjusted) the capacitor (sample) would slowly charge. Thus it was expected that pulsed extraction might require continual small changes in the pulse ratio (charge chasing) to maintain the sample within the desired electrostatic potential range. No evidence of charge chasing appeared, but changes in pulse ratio did change the relative amplitudes of the positive and negative ion spectra. Clearly there were other mechanisms involved. Over time, differences in pulsed extraction behavior on different SIMS instruments precipitated an investigation that uncovered the charge stabilizing mechanisms involved, and that knowledge led directly to the self-charge-stabilizing ion optics methods described below.

2. Theory

As a sample charges its electrostatic potential changes. This in turn changes the local electrostatic field around the sample. The changed electrostatic field acts to modify the trajectories of emitted and absorbed charged particles, changing the net charge flux to and from the sample (e.g. more or less charge returns to the sample). In certain cases, this process leads to a situation of self-charge-stabilization.

2.1. An introductory example

This introductory example consists of two electrodes made of conductive material (a cutaway view is shown in Fig. 1). The first electrode is a tube with a capped end that is held at an electrostatic potential of zero volts (grounded). The second electrode is a disk

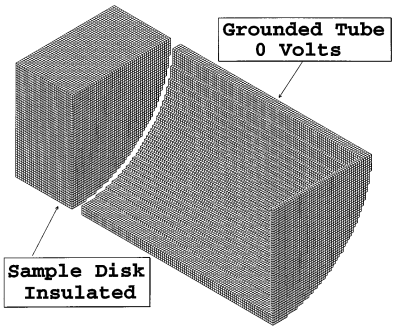

Fig. 1. Cut-away view of the SIMION model of the sample (non-conducting sample disk) and conductive grounded tube.

that serves as the sample. The conductive sample is assumed to be electrostatically insulated from its surroundings, and therefore free to seek its own potential. For the sake of discussion, it will be assumed that the initial potential of the sample is zero volts.

It is assumed that the front surface of the sample is bombarded by a primary electron beam of appropriate energy to provide a secondary electron yield (γ) greater than one: $\gamma > 1$. (The number of secondary electrons emitted from the sample exceeds the number of primary electrons colliding with the sample.) Thus there is a net outflow of negative charge from the sample causing it to charge in the positive direction. When the sample's electrostatic potential becomes more positive relative to the zero volt potential of the grounded tube, a localized electrostatic potential energy well forms around the sample. As the electrostatic energy well deepens a percentage of the lower energy secondary electrons cannot escape and are reflected back onto the sample. This reduces the net charge flux imbalance and thus slows the charging rate.

Eventually the sample will self-charge-stabilize at a potential where the potential energy well for secondary electrons is sufficiently deep to cause a net charge flux balance. Fig. 2 demonstrates how a potential energy well for secondary electrons can promote charge flux balance on the sample. Note: This is an electron's view of the potential energy world. Negative potential is up and positive potential is down.

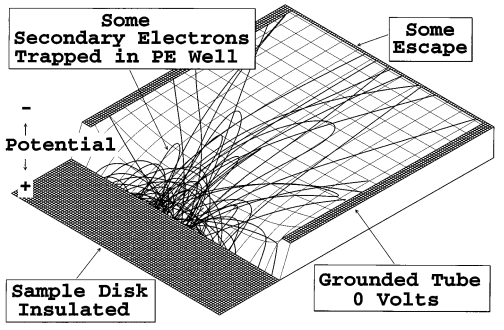

Fig. 2. Potential energy surface display of the trajectories of secondary electrons emitted from the sample disk. The potential field is indicated by the net-like grid.

The magnitude of the sample potential required for net charge flux balance is determined by the secondary electron yield, the secondary electron energy spectrum and the geometry of the electrodes (tube and sample) that create the fields. If the secondary electron yield is perturbed slightly (with γ remaining $>$ 1), the induced sample charging changes the potential energy well to automatically restore net charge flux balance.

The amount that the sample's potential must change to re-establish charge balance is dependent on the secondary electron energy spectrum. If it is assumed that all of the secondary electrons have energies less than one eV, the sample's potential would only need change a fraction of an eV. However, since the secondary electrons have a wide range of energies, one would expect that perturbations in the secondary electron yield could result in significant shifts in sample balance potential.

If the secondary electron yield is less than one ($\gamma < 1$), the sample will start to charge in the negative direction, because more primary electrons are impacting the sample than secondary electrons are being emitted. In this case a potential energy ridge (instead of a well) will form for secondary electrons. This ridge prevents emitted secondary electrons from returning to the sample, and thus no self-charge-stabilizing field is formed and the charging of the sample continues toward increasingly negative potentials. The negative charging limit occurs when the negative potential of the sample prevents all primary electrons from reaching it.

2.2. Applying these insights to real observations

The above introductory example of self-charge-stabilization can provide a useful perspective for real observations. In the case of charge compensation via electron flood, it has been found that improved charge compensation results when the electron flood beam is directed toward an alternate target close to the sample rather than the sample itself [4]. From the model it is apparent that the alternate target and the sample form an electrostatic servo loop with low energy secondary electrons from the alternate target providing the self-charge-stabilization. In this case, the sample is assumed to be initially charged positive. The low energy secondary electrons are attracted to the sample. This starts the sample charging in the negative direction. As the sample charges more negative than the alternate target, fewer secondary electrons can make the journey to the sample. The potential of the sample then self-charge-stabilizes relative to the alternate target. The use of the alternate target provides a potential reference for the sample and the low energy secondary electrons are sacrificed to provide the self-charge-stabilizing servo. Sample charging is easier to control, because small shifts in sample potential now dramatically impact the trajectories of the low energy secondary electrons produced at the alternate target.

2.3. Implications of impact energy dependent secondary electron yields

In the introductory example above, secondary electron yield is assumed to be constant. Actually, secondary electron yield is a function of the sample material and the impact energies of the primary electrons, as shown in Fig. 3. If the primary electron energies are low enough (below 0.25 keV) the secondary electron yield is less than one ($\gamma < 1$), causing the sample to charge in the negative direction. As the sample charges more negatively, primary electrons must climb a potential hill to hit the sample and their

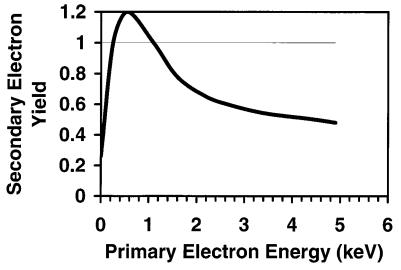

Fig. 3. Typical secondary electron yield from a metal oxide as a function of primary electron impact energy.

impact energies are reduced. However, the secondary electron yield decreases with reduced primary electron impact energy in this region of the secondary electron yield curve. Therefore the sample will charge to its negative charging limit as described above.

For primary electron energies between 0.25 keV and 1.1 keV, the secondary electron yield is greater than one (Fig. 3) and the self-charge-stabilizing potential controls sample charging as described above. The electrode geometry design of Fig. 1 keeps the sample's potential within a few volts of ground for secondary electron yields up to 1.3. Thus, the *effective* secondary electron yield is essentially held constant by self-charge-stabilization mechanisms within this range.

Electron primary beam energies above 1.1 keV move the operating point into the upper region of the yield curve where the yield is less than one ($\gamma < 1$). This causes the sample to charge in the negative direction. However as the sample charges more negative the primary electrons have to climb an increasingly higher electrostatic hill to hit the sample. This reduces their impact energies, and improves their secondary electron yields. Negative charging will continue to the point where the effective secondary electron yield equals one. The sample is now stabilized at its electron yield self-charge-stabilizing potential.

Perturbing the sample to a more positive potential would increase the primary electron impact energy. The secondary electron yield would shift to be somewhat less than one and the sample would charge in the negative direction to restore the electron yield self-charge-stabilizing potential. Perturbing the sample's potential in the negative direction is a more complex situation. If the perturbation of the sample's potential is small enough so that the primary electrons still impact within the range of effective energies where secondary electron yield is greater than one (0.25 keV to 1.1 keV), then the sample's potential will self-restore to its electron yield self-charge-stabilizing potential. However, if the negative potential perturbation is large enough to lower the impact energies to a point where secondary electron yield is less than one (below 0.25 keV), self-charge-stabilization control will be lost, and negative charging of the sample will continue up to the negative charging limit. Moreover, if the negative sample potential is perturbed beyond the negative charging limit the sample's new potential will remain unchanged because there are no primary electrons that have enough energy to reach it.

2.4. A more complex example: positive and negative ion emission

Self-charge-stabilizing mechanisms become more complex when charge is transported away from the sample by positive and negative secondary ions as well as secondary electrons. The following example introduces bi-polar self-charge-stabilizing mechanisms, and requires one to mentally flip between positive and negative potential energy surfaces. This is roughly equivalent to playing golf on both the upper and lower surfaces of a thin undulating sheet.

The bi-polar self-charge-stabilizing effect is demonstrated with an idealized system where a high energy primary beam impacts a thin sample causing the emission of positive and negative secondary ions. The sample is suspended (magically) in the middle of a linear gradient field as shown in Fig. 4. The sample is assumed to be electrically isolated so it is free to seek its own potential subject to the effects of the gradient field and the inflow and outflow of charged particles from its surface.

For initial simplicity we assume the bombarding beam is neutral, an equal number of positive and negative secondary ions are emitted from the sample, and no secondary electrons are emitted. An electro-

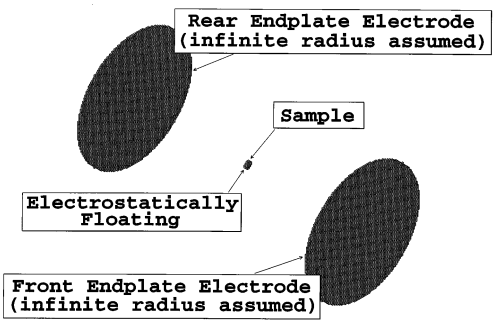

Fig. 4. Idealized model of a non-conducting sample suspended between conductive plates for illustrating self-charge-stabilizing mechanisms.

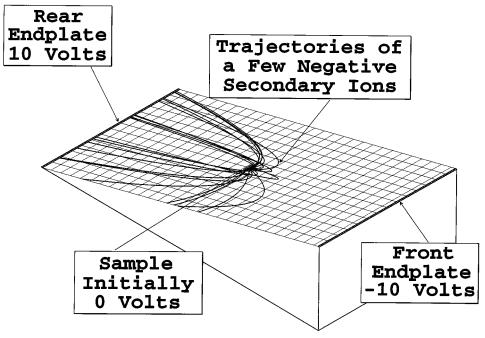

Fig. 6. Negative ion potential energy surface view of the non-conducting sample (at 0 V) in a linear gradient field showing a few representative negative ion trajectories.

static gradient is established by setting the rear endplate electrode to +10 V and the front endplate electrode to −10 V. If the sample's front face is placed midway between the endplates, the electrostatic potential at that location will be 0 V. The sample's electrostatic potential starts at 0 V (minimizing the field perturbations around the sample) as shown in the positive ion potential energy surface view in Fig. 5. Initially all of the positive secondary ions are extracted toward the front endplate electrode (Fig. 5), while the negative secondary ions are repelled back toward the sample and rear endplate electrode (Fig. 6).

Because some of the negative secondary ions, but none of the positive secondary ions, return to the sample's surface, the sample will start to charge in the negative direction. As the potential of the sample becomes more negative, the near-field gradients change, forming a diverging electrostatic ridge for negative ions (Fig. 7). As the sample charges more negative, the near-field electrostatic ridge increases, and its diverging character reduces the percentage of negative ions that return to the sample, slowing the sample's negative charging rate.

The impact on positive secondary ions is just the reverse. As the sample charges in the negative direction, a converging electrostatic near-field well forms in front of the sample and acts to block the exit of the lowest energy positive secondary ions. As the near-field well deepens a higher proportion of positive secondary ions are reflected back onto the sample, further slowing the negative charging rate. The sample will continue to charge in the negative direction

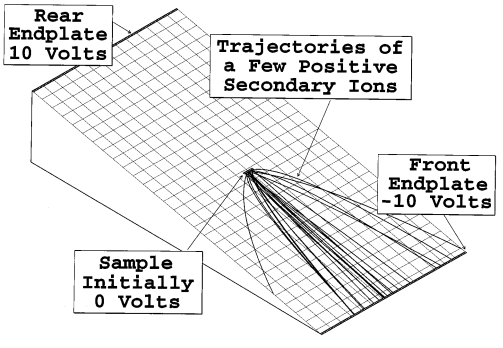

Fig. 5. Positive ion potential energy surface view of the non-conducting sample (at 0 V) in a linear gradient field showing a few representative positive ion trajectories.

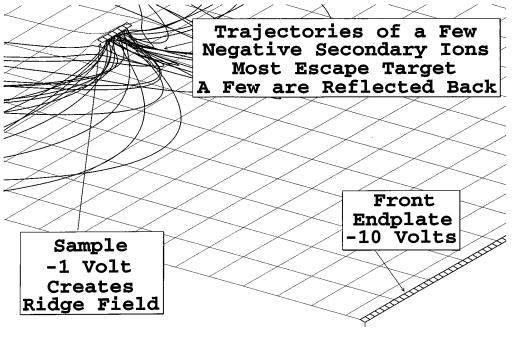

Fig. 7. Close-in view of the negative ion potential energy surface with the sample at −1 V, demonstrating the formation of a near-field ridge at the sample, and the effect on the trajectories of a few negative ions emitted from the sample.

until the same average number of negative and positive secondary ions return to the sample. The sample's potential will stabilize at that point because the net flux of charge is zero.

This flux balance potential is self-restoring. If the electrostatic potential of the sample is perturbed in either direction the resulting changes in the electrostatic near-field will automatically induce sample charging that restores the flux balance potential. Moreover, changing the relative numbers of positive and negative secondary ions emitted will cause an automatic shift toward a new flux balance potential that maintains charge flux balance for the changed secondary ion emission profile. Clearly the field gradients and the kinetic energy spread of the secondary ions will effect the flux balance potential. Simulations were performed to investigate the relative importance of these parameters, and gain insights that might assist in designing ion extraction optics.

3. Simulations

Simulations were performed using the user program facility of SIMION 3D [5]. The simulations studied the interaction between electrode geometry, electrode potentials, and the flux of charged particles that impact on or are emitted from the sample. The objective was to determine the sample potential for net flux balance given the initial conditions specified (e.g. electrode geometry, potentials, initial charge flux, and energy spectra of the various charged particles). This was accomplished by guessing a sample potential, simulating a period of randomized charge emission, computing the charge balance, guessing a new sample potential, and rerunning the simulations until charge balance was obtained.

The sample was held at a fixed potential for each iteration of a simulation. Each Monte Carlo style iteration randomly emitted 300 to 2,000 secondary ions and electrons (depending on the simulation) from the surface of the sample. Initial sample charging, the emission of charge via secondary particles, and any return of charge via the return of secondary particles repelled back onto the sample were automatically tracked. This information was then used to obtain the net sample charge for each iteration. A binary approach algorithm used the net sample charge information to obtain a new sample potential estimate to use in the next iteration. These iterations were repeated (re-randomized and re-flew the emitted secondary particles, recalculated the net sample charge, and re-estimated the sample potential) until a defined convergence limit of charge flux balance was obtained.

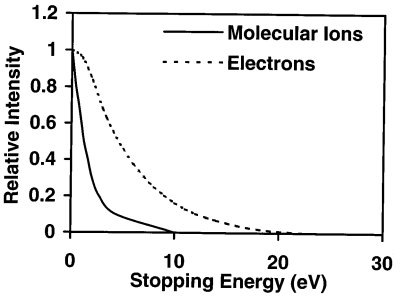

Fig. 8. Stopping energy distributions for molecular ions and electrons used in the SIMION simulations.

Secondary particles were re-randomized on each successive iteration of a simulation in the following manner. Each secondary particle had an equal probability of being emitted at any radius circle from the center of the circular sample to its edge. This biased the emission density toward higher emission at the center of the sample. However, subsequent uniform area emission probability simulations gave essentially the same results. The angles of emission were equal probability in elevation ($+89°$ to $-89°$) and azimuth (0°–360°) to a line normal to the sample surface passing through the point of actual particle emission. Secondary ion energies were randomized using a sixth order polynomial fit of secondary molecular ion emission data published in [6]. Secondary electron energies were randomized using a sixth order polynomial fit of secondary electron emission data from Benninghoven [7]. The stopping energies used for secondary particles in these simulations are shown in Fig. 8.

A series of simulations was made for the simple model described above. The first collection of simulations was made to compare the sample balance

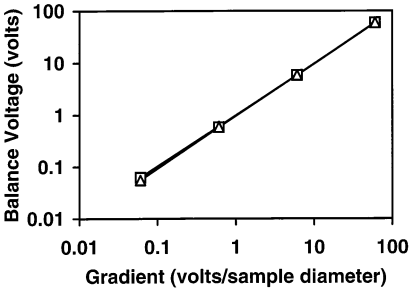

Fig. 9. Calculated balance offset potential (voltage) as a function of the normalized potential gradient between the endplates of the model.

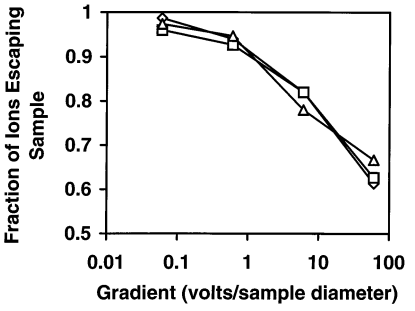

Fig. 10. The fraction of the secondary ions that are successful in escaping the sample as a function of the normalized potential gradient between the endplates of the model.

offset potential to the overall field gradient. The sample balance offset potential represents the sample's potential offset from the zero volt potential the sample would be at if its potential was in nominal equilibrium with the gradient field created by the two endplates. As such it is a direct indication of the magnitude of the localized ridge/well field around the sample. The results shown in Fig. 9 show that balance offset potential (voltage) increases linearly with potential gradient. Note: The potential gradient has been normalized to the sample diameter to facilitate scaling. There are three series simulating identical conditions represented in Fig. 9. They serve to demonstrate that simulations of identical conditions generally gave very consistent balance offset potential results.

It is important to note that most of the secondary ions normally escape from the sample. Generally, only the lower energy secondary ions are recaptured to maintain charge flux balance. Fig. 10 shows the fraction of the secondary ions that are successful in escaping the sample. Notice that the percentage of escaping secondary ions increases as the potential gradient decreases. Over 90% of the secondary ions of both polarities escape the sample for the lower potential gradients. This is logical because the lower gradients produce lower balance offset potentials, and lower balance offset potentials result in shallower potential well fields that trap fewer charged particles. In general, it is highly desirable to minimize the percentage of secondary ions that are required to achieve charge balance in order to maximize the percentage of secondary ions that are available for detection. Low field gradients near the sample can help to realize this goal. However, it is important not to draw too many hard conclusions from Figs. 9 and 10 as they represent a very idealized system. More realistic simulations complicate the picture considerably.

4. The charge flux balance equation

In order to proceed to more complex simulations of self-charge-stabilization mechanisms it is necessary to introduce the charge flux balance equation:

$$\mathrm{Flux}_{\mathrm{Avg}} = 0$$

$$= \mathrm{Flux}_{\mathrm{Primary}} + \mathrm{Flux}_{\mathrm{Emitted}} + \mathrm{Flux}_{\mathrm{Returned}}$$

The average charge flux on the sample ($\mathrm{Flux}_{\mathrm{Avg}}$) is the sum of the charge flux from the primary particle beam ($\mathrm{Flux}_{\mathrm{Primary}}$), the charge flux from emitted secondary charged particles ($\mathrm{Flux}_{\mathrm{Emitted}}$, e.g. electrons and secondary ions), and the charge flux returned by secondary charged particles that are reflected back onto the sample's surface ($\mathrm{Flux}_{\mathrm{Returned}}$). When the average flux is zero the sample is charge balanced (has a stable potential).

5. Effects of secondary electrons

Secondary electron emission complicates the situation in that the secondary electron energy spread is

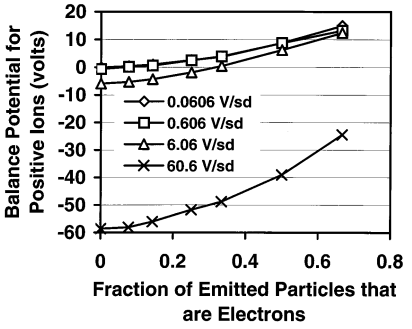

Fig. 11. Calculated flux balance potentials obtained when extracting positive ions for varying fractions of electron emission (as a fraction of the total secondary charged particle emission) for four different field gradients (volts/sample diameter).

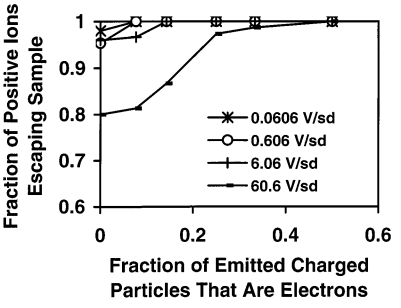

Fig. 12. Calculated fraction of positive ions escaping from the sample as a function of the fraction of emitted charged particles that are electrons for four field gradients (volts/sample diameter).

much broader than that of the secondary ions, and generally more secondary electrons are emitted than secondary ions. However, in order to achieve charge flux balance, the sum of the emitted secondary charge flux and the returned charge flux must still be zero (neutral primary beam assumed):

$$\text{Flux}_{\text{Avg}} = 0 = \text{Flux}_{\text{Emitted}} + \text{Flux}_{\text{Returned}}$$

The added emission of secondary electrons causes the sample's potential to shift in the positive direction. As the potential shifts more positive, a potential well field forms for negatively charged particles, capturing the lower energy negative particles. At the same time, this deepening potential near-field well acts as a rising near-field ridge for positive ions, reducing their reflection back onto the sample. The overall result has different implications for negative and positive ion detection.

Fig. 11 shows the flux balance potentials obtained when extracting positive ions for varying percentages of electron emission (as a fraction of the total secondary charged particle emission) for four different field gradients. As the flux balance potential shifts more positive (with increasing percentages of secondary electron emission), the potential near-field well for positive ions switches into a potential near-field ridge, and all positive ions start escaping successfully, a plus if detection of positive ions is the objective. This effect is demonstrated in Fig. 12.

The extraction of secondary negative ions is not so favorable. As increasing percentages of secondary electrons are emitted, the positive shift in flux balance potential (Fig. 13) deepens the potential near-field well for negatively charged particles, forcing more of them to return to the sample. Unfortunately, secondary negative ions (particularly secondary negative molecular ions) are generally less energetic than secondary electrons. Thus a disproportionate number of secondary negative molecular ions are sacrificed (captured in the well) while the secondary electrons escape. Fig. 14 shows the dramatic fall off of secondary negative molecular ion emission as secondary electron emission increases.

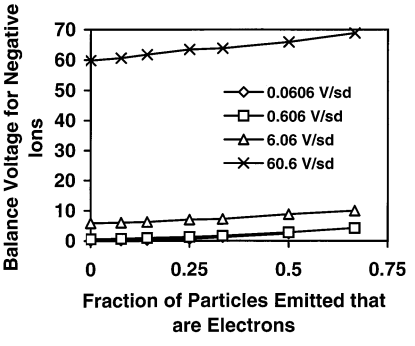

Fig. 13. Calculated flux balance potentials obtained when extracting negative ions for varying fractions of electron emission (as a fraction of the total secondary charged particle emission) for four different field gradients (volts/sample diameter).

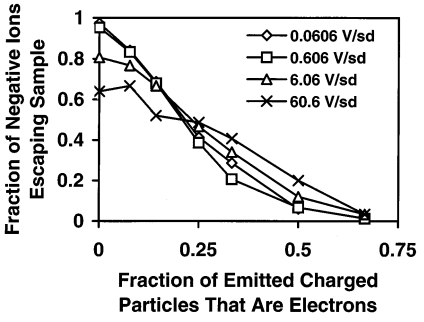

Fig. 14. Calculated fraction of negative ions escaping from the sample as a function of the fraction of emitted charged particles that are electrons for four field gradients (volts/sample diameter).

6. Including the effects of primary beam charge

Non-neutral primary beams further complicate the situation by transporting charge directly onto the sample. Since the kinetic energy of the primary beam particles is generally much higher than the range of sample potentials, the primary beam flux is independent of the sample potential. Therefore, in these simulations the primary beam flux was assumed to be constant.

6.1. Positive ion primary beams

Positive ion primary beams are commonly used in SIMS. However, the positive primary beam flux induces positive charging. Moreover, any negative secondary ions and secondary electrons that escape from the sample also induce positive charging. Only the positive secondary ions that escape from the sample act to reduce this positive charging. Unfortunately, the net result is often strong positive charging that complicates the self-charge-stabilization process.

Positive sample charging forms a potential near-field ridge for positive secondary ions and potential near-field well for negative secondary ions and secondary electrons. Even if the potential well for negative secondary ions and secondary electrons were deep enough to reflect them all back to the sample (to stop their positive charging effect), the primary beam would still continue to charge the sample in the positive direction (ignoring for the moment the emission of positive secondary ions). However, once a potential near-field ridge (for positive ions) has been established, all the positive secondary ions are already escaping. Unless the positive secondary ion yield is greater than one ($\gamma > 1$), the sample cannot self-charge-stabilize. Unfortunately, positive secondary ion yields are almost universally much less than one. This is why insulating samples tend to charge uncontrollably positive when irradiated with a positively charged primary beam.

The most common method employed to control this form of positive charging is to flood the sample directly with relatively low energy electrons. Once the appropriate flux of electrons is flooding the sample, self-charge-stabilization processes resume and the sample's potential stabilizes. If the electron flood beam were perfectly adjusted, the sample's offset potential should stabilize to near zero volts (using the above simulation model).

However, if slightly too many electrons flood the sample, the sample will charge in the negative direction. This negative charging forms a potential well for positive secondary ions. The lowest energy positive secondary ions are sacrificed first (mostly positive secondary molecular ions) to achieve self-charge-stabilization. Further increases in the electron flood excess causes an increasing percentage of positive ions to be trapped in the potential well until all positive secondary ions are trapped and self-charge-stabilization is lost. The sample then charges negatively, raising the potential hill seen by the electron flood beam, reducing the numbers of incoming electrons hitting the sample, until charge flux balance occurs. This assumes that the energies of the flooding electrons are sufficiently high to force total positive secondary ion trapping before significant electron flood attenuation occurs. If this is not the case, the two processes will overlap.

The excess of flood electrons leads to the creation of a potential well field for positive secondary ions. This well field acts to reduce the number of positive secondary ions that escape. However, the potential energy well for positive ions acts as a potential energy ridge for negative secondary ions and secondary electrons. The negative secondary ion ridge field

insures that virtually all negative secondary ions successfully escape the sample.

Conversely, if the electron flood beam intensity is reduced below optimum, the sample will charge in the positive direction. A potential energy ridge field is created for positive secondary ions (all positive secondary ions escape), and a potential energy well field is created for negative secondary ions and secondary electrons (some negative secondary ions and secondary electrons are trapped). As the electron flood deficit increases, the potential well eventually deepens to the point where all negative secondary ions and secondary electrons are trapped. At this point self-charge-stabilization is lost and the sample charges uncontrollably in the positive direction.

The adjustment of the electron flood beam intensity and kinetic energy can be non-trivial. There is a relatively narrow intensity range (percentage wise) where self-charge-stabilization is obtained. If the electron flood beam kinetic energy is too high, sample potential swings are enhanced. Moreover, potential ridge and well fields reverse when crossing the optimum and vary in magnitude within the range of self-charge-stabilization. The self-adjusting ridge and well fields act to change the emitted secondary ion intensities and can suppress emission of the lower energy secondary molecular ions.

These problems can be reduced if an alternate target for the electron flood beam is used to form a low energy electron flood servo loop as described previously. If the electron flood beam is directed to an alternate target close to the sample, control and stability should improve (as discussed earlier). Self-charge-stabilization improves because the amount of secondary electron flux reaching the sample from the alternate target is more sensitive to changes in sample potential.

6.2. Negative ion primary beams

Negative ion primary beams tend to compensate for the excess negative charge leaving the sample in the form of secondary electrons. Thus negative ion primary beams act to mitigate the sample's charge imbalance rather than aggravating it as positive ion primary beams generally do.

Our group uses a Perrhenate (ReO_4^-) negatively charged heavy molecular primary ion beam in our SIMS instruments [8]. It has worked quite well, in conjunction with the self-charge-stabilizing designs these instruments employ, with virtually all the insulating samples we have tested [9,10] without the need to make use of ancillary charge flood beams of either polarity.

7. Self-charge-stabilization with leakage rings

The discussion thus far has been limited to idealized electrode configurations. This has served to demonstrate the mechanisms of self-charge-stabilization. However, the choice of electrode geometry plays a significant role in how well the self-charge-stabilizing process actually works in practice. The most important design goal should be to self-charge-stabilize the sample by sacrificing the minimum percentage of secondary ions that could otherwise be extracted for detection.

The most demanding objective would be to extract the maximum number of secondary ions of both polarities for simultaneous detection. This requires that the sample be maintained within a volt or two of the detection inlet, and that any potential energy wells remain as shallow as possible. These goals are best accomplished with electrode geometry designs that create very low potential gradients near the sample while exerting tight control over sample potential excursions. It is also extremely helpful if the net charge flux is intrinsically close to being charge balanced (e.g. via the use of a negative primary ion beam like ReO_4^-).

A less demanding objective would be to extract the maximum number of secondary ions having a designated polarity. This generally requires that the sample's potential assists the far-field's potential gradient in directing the designated polarity secondary ions into the detection inlet (e.g. the sample's potential is part of a far-field downhill run for the designated polarity secondary ions). Further, it is highly desirable

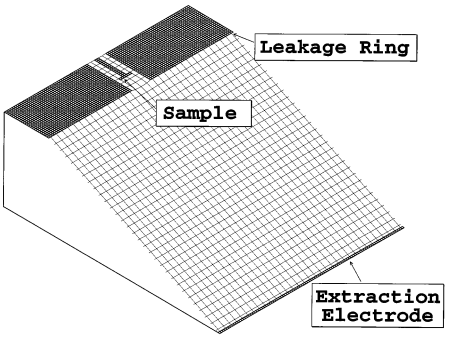

Fig. 15. SIMION model of the leakage ring geometry shown as a potential energy surface as seen by an ion attracted to the extraction electrode.

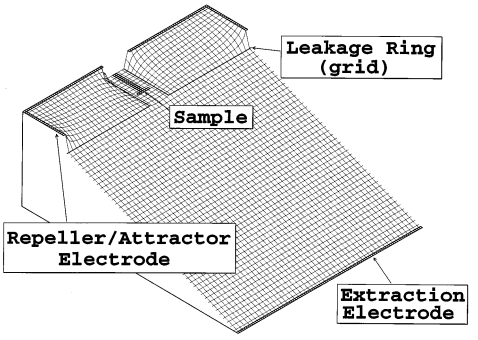

Fig. 16. SIMION model of a low-loss leakage ring design.

that the self-charge-stabilization process not create a near-field potential energy well for the designated polarity secondary ions. This condition is best satisfied when a small near-field ridge exists for the designated polarity secondary ions at charge balance (forcing them away from the sample). These goals are best accomplished with electrode geometry designs that create relatively low potential gradients near the sample while exerting moderate control over the sample's potential. Moreover, it is advantageous to have a slight excess emission of opposite polarity charge (e.g. a slight excess emission of negative charge ($Flux_{Emitted} < 0$), when positively charged ions are being extracted for detection) to help create a near-field ridge at the self-charge-stabilization potential.

A relatively simple electrode geometry appears to provide most of these desirable characteristics. This electrode geometry is called a leakage ring, and we employ it for self-charge-stabilization in all of our Ion Trap SIMS instruments [11,12]. Fig. 15 shows a leakage ring in its simplest embodiment as a potential energy surface for the ion of the extracted polarity. The leakage ring is a thick electrode with a hole drilled through it and the sample is recessed within the hole. The sample assembly (pin and head) should be conductive, but must be electrically insulated from the rest of the sample probe so it can track the sample surface's potential. It is advantageous that the sample assembly have minimal capacitance to speed its tracking of the sample surface potential.

Note in Fig. 15 that the electrostatic field gradients are very shallow near the sample. Shallow gradients maximize the percentage of charged secondary particles (of both polarities) that successfully escape the sample, and thus minimize the percentage of charged secondary particles that return to the sample to establish self-charge-stabilization. Simulations with the example in Fig. 15 indicate that the sample self-charge-stabilizes its potential within 0.1 volt of the leakage ring's potential when the potential difference between the leakage ring and extraction electrode is 100 V (assuming equal positive and negative secondary charge is emitted: $Flux_{Emitted} = 0$). If the emitted flux is not initially zero (e.g. secondary electrons are emitted: $Flux_{Emitted} < 0$), the sample's potential will settle to a non-zero offset potential from the leakage ring (offset potential = sample potential–ring potential) that forces net charge flux balance. The deeper the sample is recessed in the hole, the more constant this offset potential will become (less affected by changes in the leakage ring's potential). However, a solid leakage ring also acts to scavenge secondary particles of either polarity, and the deeper the sample is recessed, the higher the percentage of ions lost to the leakage ring. Simulations of the leakage ring geometry of Fig. 15 indicate that only about 30% of the extracted secondary ions reach the extraction electrode at charge balance.

Modification of the leakage ring design can improve the extracted secondary ion yield. Fig. 16 shows a leakage ring made of a flat grid with a tubular grid surrounding the sample (made with lengthwise wires

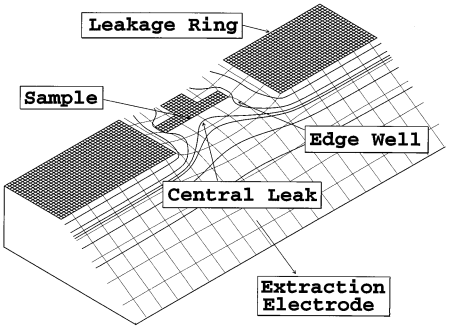

Fig. 17. Calculated near-field potential energy surface surrounding a shallow-depth leakage ring sample.

to minimize low angle ion blockage). The sample is placed within the tubular grid. Behind the flat grid (labeled leakage ring grid in Fig. 16) is a repeller/attractor electrode that acts to repel the secondary ions of the extracted polarity and attract the secondary ions of the opposite polarity. The grids and repeller electrode allow over 95% of the extracted secondary ions to reach the extraction electrode.

Fig. 17 illustrates an alternate design approach that locates the sample at a shallow depth in the leakage ring. This makes the potential of the extraction electrode more visible to the sample (increasing charge balance offset potential to about 1 V simulation of Fig. 17's geometry). Fig. 17 illustrates the near-field around the sample at charge balance. Notice that the locally strong convergence field tends to focus the extracted ions toward the extraction electrode. This field, along with the sample's shallow recess depth in the leakage ring, allows approximately 75% of the extracted ions to reach the extraction electrode. Further, the potential energy well is shaped like a torus that surrounds a sample central leak area. If the primary beam uniformly exposes all areas of the sample, low energy secondary ions from the sample's outer radial areas provide the self-charge-stabilization, allowing the low energy secondary ions emitted near the sample's center to escape through the central leak (central secondary ions have a slight ridge field). Moreover, the reflected secondary ion trajectories allow some of the reflected secondary ions to impact the center area of the sample, and perhaps help

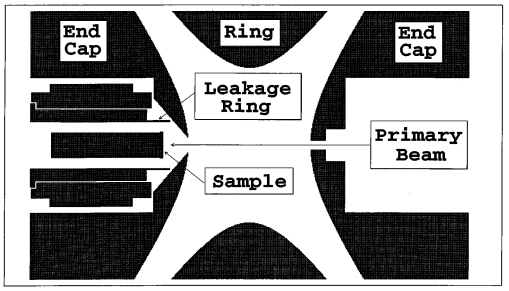

Fig. 18. SIMION model of the as-built ion trap SIMS with a leakage ring charge compensation system.

mitigate the sample's central charge loss due to the central leak (reducing undesirable central region charging of the sample). The shallow depth leakage ring design has proven to be quite effective for sample charge compensation in our Ion Trap SIMS instruments. The leakage ring equipped Ion Trap SIMS was used in experiments to isolate and evaluate self-charge-stabilization effects as described below.

8. Experimental

Evidence of the behavior of self-charge-stabilizing mechanisms has been obtained by investigating a self-charge-stabilizing leakage ring design on an ion trap SIMS. Fig. 18 shows a cross-sectional view of the ion trap with its installed leakage ring assembly. A 5 keV 100 pA Perrhenate negative ion primary beam was directed right to left along the axis of the trap through the center of both end caps to the sample.

8.1. Measurements of intrinsic offset potentials

If the sample were recessed deep within the leakage ring, the sample's view of the world would be dominated by the leakage ring's potential. Self-charge-stabilizing mechanisms, if active, would be expected to keep the sample's balance potential at a fixed difference (or offset) from the leakage ring's potential.

Measurements of the intrinsic offset potentials of a conductive stainless steel sample relative to various leakage ring potentials were made with the sample

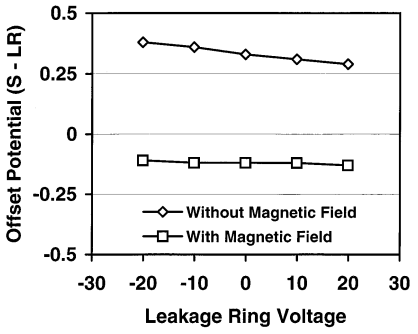

Fig. 19. Measured sample offset potentials as a function of leakage ring voltage with and without a 30 Gauss transverse magnetic field applied to the sample region.

positioned at a 10.2 mm depth from the front edge of the leakage ring (Fig. 18 shows a more typical 1.3 mm sample depth from the front of the leakage ring). The 5 keV 100 pA Perrhenate negative ion primary beam was turned on, the trap Rf was turned off, and the potential of the conductive stainless steel sample (dirty) was measured with an electrometer for a series of leakage ring potentials from −20 to 20 V. The sample's offset potential was then calculated with the following formula:

$$\text{Sample Offset Potential} = \text{Sample Potential} - \text{Leakage Ring Potential}$$

Fig. 19 compares sample offset potential as a function of the leakage ring potential. The offset potential averaged 0.34 V (upper trace). It is interesting to note that the sample's offset potential remained positive during these observations (upper trace varies from 0.38 to 0.29 V). This indicates that there was an initial excess emission of negative secondary charge from the sample. The initial excess negative emission caused the sample to charge positive relative to the leakage ring potential. The sample's positive offset potential then created a near-field potential energy well sufficiently deep to retain all the excess negative charge (reducing the net flux to zero).

The positive offset potential also indicates that a near-field ridge was formed for positive secondary ions (all escaped). This would be the desirable situation for extracting positive secondary ions. However, the consequential near-field potential energy well for negatively charged particles traps low energy negative secondary ions and electrons. This would not be the most desirable situation for extracting negative secondary ions, particularly lower energy molecular negative secondary ions.

In order to shift the sample's offset potential from positive to negative, a magnetic field was employed to increase the percentage of secondary electrons that returned to the sample (lower trace, Fig. 19). A permanent magnet was positioned outside the trap's vacuum chamber to create a transverse magnetic field across the sample's surface. The magnetic field's strength at the sample's face was measured to be 30 Gauss by a Hall probe. Fig. 19 shows the sample offset potentials as a function of leakage ring potential when the magnetic field was present. The addition of a 30 Gauss magnetic field switched the sample's offset potential from an average of 0.34 to −0.12 V.

The negative offset potential indicates that the magnetic field caused enough secondary electrons to return to the sample that a slight excess emission of positive secondary charge was created. The negative offset potential caused a small near-field ridge to form for negative ions (all escaped), and a near-field potential energy well for positively charged ions to form that returned the excess positive charge emission back to the sample. The use of magnetic fields to suppress secondary electron emission serves as a practical example of one way to manipulate the intrinsic emission ratio of secondary charge to obtain more desirable near-field characteristics for the extracted ion polarity. This has been employed in some experimental systems [13].

These observations confirm that self-charge-stabilizing mechanisms are controlling the sample's potential. At the 10.2 mm sample depth, charge balance is controlled primarily via secondary ion and secondary electron interactions with the leakage ring. The sample's potential should shift to establish a potential difference, or offset potential, relative to the leakage ring that achieves net flux balance. When the potential of the leakage ring is changed, the sample's potential should automatically shift to restore the same offset potential that previously maintained net flux balance.

Thus sample offset potential should not be a function of leakage ring potential for these experimental conditions.

The observed sample offset potentials were relatively constant when the 30 Gauss magnetic field was active. However, the observed non-magnetic field sample offset potentials had a slight slope (0.37 to 0.29 V) for a range of leakage ring potentials (−20 to 20 V). These observations can be explained if one assumes that a small flux of low energy electrons accompanied the primary beam. The source of these primary electrons appeared to be the edges of an upstream primary beam collimator. The weak magnetic field would act to deflect these electrons away from the sample. Thus when the magnetic field was active the sample offset potentials should be more constant, because few if any of these primary electrons ever hit the sample. However, when no magnetic field was active the percentage of primary electrons that would hit the sample would be a function of the sample's potential. Negative sample potentials (caused by negative leakage ring potentials) would reduce (via repulsion) the numbers of primary electrons that hit the sample. This would cause the sample offset potential to shift positive to more closely approach its intrinsic (primary electron free) offset potential. Positive sample potentials (caused by positive leakage ring potentials) increase (via attraction) the numbers of primary electrons that hit the sample. This would cause the sample offset potential to shift more negative.

8.2. Impact of near-field ridges and wells on ion spectra

An experiment was also conducted to discern what impact a 30 Gauss magnetic field would have on the secondary ion spectra of a conductive Rhenium sample. The intrinsic offset potential for the Rhenium sample was found to be 0.45 V (no magnetic field) and −0.2 V (with a 30 Gauss magnetic field) using the technique described above. The Rhenium sample was set to a depth of 6.4 mm from the edge of the leakage ring. This sample location served as a compromise between the need to maintain deep leakage ring control of the sample's offset potential and the need to observe secondary ion spectra via the ion trap.

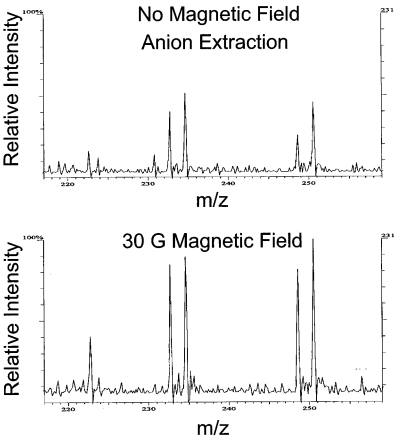

Fig. 20. ReO_4^- (*m/z* 233, 235) and ReO_4^- (*m/z* 249, 251) secondary ion signals obtained without (top) and with (bottom) a 30 Gauss transverse magnetic field applied to the sample region.

The leakage ring was set to a potential of −15 V forcing a negative sample potential to induce injection of negative secondary ions into the ion trap. Fig. 20 shows a range of negative secondary molecular ion peaks with and without a magnetic field applied. Note that the intensity of these peaks approximately doubled when the magnetic field was turned on. The magnetic field switched the near-field potential well to a potential ridge for negative secondary ions. This allowed more negative secondary ions to escape the sample, giving rise to the more intense ion peaks observed.

The leakage ring was then set to a potential of 20 V forcing a positive sample potential to induce injection of positive secondary ions into the ion trap. Fig. 21 shows the positive secondary molecular ion peak at 149 amu with and without a magnetic field applied. Note that the intensity of this peak was reduced approximately 25% when the magnetic field was turned on. The magnetic field switched the near-field potential ridge to a potential well for positive ions. This acted to trap the lower energy positive secondary ions at the sample, reducing the observed peak intensities.

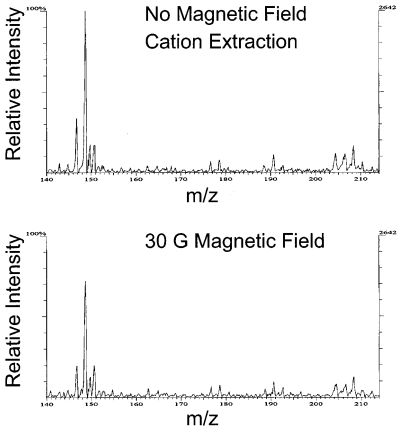

Fig. 21. Phthalate (*m/z* 149) molecular ion signals obtained without (top) and with (bottom) a 30 Gauss transverse magnetic field applied to the sample region.

The above observations provide experimental evidence that the character of self-charge-stabilizing near-fields does impact secondary ion spectra.

8.3. Primary beam kinetic energy and offset potential

An experiment was conducted to observe the changes in the offset potential of a stainless steel sample as a function of primary beam kinetic energy. A stainless steel sample was recessed at a 10.2 mm depth from the front edge of the leakage ring to isolate it from external fields. Offset potentials were then measured for Perrhenate primary beam kinetic energies from 3 to 9 keV as shown in Fig. 22. The stainless steel sample was removed from the vacuum system and rinsed with acetone before each run (to restore the initial surface character).

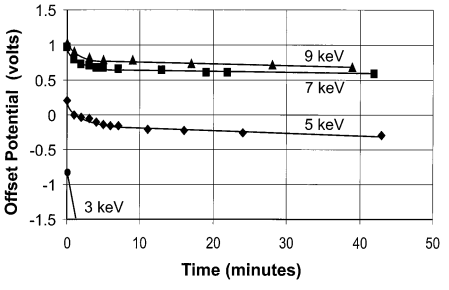

Fig. 22. Offset potentials as a function of exposure time measured for primary beam kinetic energies from 3 to 9 keV.

The initial offset potential (time = 0) varied from −0.8 V at 3 keV to 1.0 V at 9 keV primary beam kinetic energies. The results indicate that yields of secondary electrons and perhaps the yields of secondary ions increase with higher primary beam kinetic energies (within the kinetic energy range observed) for stainless steel, pushing the offset potential more positive. The ability to vary sample offset potential by changing primary beam kinetic energy provides a direct way to control the charge balance operating point (e.g. induce a near-field ridge for the extracted particle polarity).

8.4. Secondary ion emission stability

The above observations were continued for approximately 40 minutes to examine the temporal stability of the offset potentials (Fig. 22). It appears these samples had surface contaminates that initially increased the net emission of negatively charged secondary particles and/or initially reduced the emission of positive secondary ions (resulting in initially more positive offset potentials). Gradually, over the first 10 min, the primary ion beam cleaned off the surfaces (at a sputter rate of approximately 100 s per monolayer), reducing the apparent excess negative charge emission. This cleaning action shifted the offset potentials toward more negative values.

The 3 keV offset potential curve shows instability in self-charge-stabilization. Although the 3 keV offset potential was initially stable, it quickly charged negatively out of control as surface contaminates were removed. This indicates that the stainless steel sample's secondary electron yield at 3 keV was probably too low to support self-charge-stabilization.

The 5, 7, and 9 keV offset potential curves became relatively stable after 10 min (approximately 6 monolayers removed). The 7 and 9 keV curves maintained positive offset potentials, while the 5 keV offset potential curve settled into a negative offset potential. The 5 keV curve shows a notable downward trend while the 7 and 9 keV curves remain relatively flat.

The difference between the observed slopes can be explained by the large difference between positive and negative secondary charge emission in this system. At the flux balance potential the negative secondary charge emission must be sufficient to compensate for the primary beam negative charge influx as well as the positive secondary charge emission. The fact that positive secondary ion emission yields are commonly observed to be less than 10%, implies that the negative secondary charge emission may be over 10 times greater than the positive secondary charge emission. When the offset potential is negative, positive secondary ions are being returned to the sample to maintain charge control. A 2% shift in negative secondary charge emission could require a 20% shift (or more) in the percentage of emitted positive secondary ions that must be returned to maintain charge control. The 20% shift would require a much greater offset potential change than the 2% shift (assuming equivalent emission energy spectrums). Thus negative offset potentials would be expected to be much more sensitive to changes in secondary electron yield than would positive offset potentials (as observed). Moreover, positive offset potentials are safer than negative offset potentials in this system, because there can be a loss of self-charge-stabilization control when offset potentials are sufficiently negative (when all the positive secondary ions are returned).

These observations indicate that the sputtering ratio of positive and negative secondary particles can shift as a function of primary beam irradiation time. This is most probably due to the gradual sputtering off of atmospheric surface contaminates (hydrocarbons and the like), which gradually changes the character of the sample's surface, and consequently shifts the ratio of the positive and negative secondary charged particles that are emitted. It also confirms that self-charge-stabilization mechanisms do automatically compensate for changes in sputtering charge ratio through changes in the sample's offset potential up to the secondary emission self-control limits (100% trapping in potential energy wells).

Moreover, these observations also indicate that inducing conditions that foster an intrinsic positive offset potential (e.g. using the appropriate primary beam kinetic energy) can be an effective strategy for maintaining the stability of the sample balance potential in equivalent systems. Optimal detection of negative secondary ions would then require switching on a magnetic field of appropriate intensity to shift the offset potential slightly negative.

9. Discussion and conclusions

The use of self-charge-stabilizing leakage rings in conjunction with a negative ion primary beam like ReO_4^- has proven to be an effective charge compensation strategy for our group's ion trap SIMS instruments. Our most significant discovery has been the important role that self-adjusting near-field ridges and wells play in secondary ion and secondary electron emission, and that the character of these near-fields can be successfully manipulated (e.g. by electrode design, changes in primary beam kinetic energy, and by using magnetic fields). For example, a magnetic field can be used to selectively recapture secondary electrons, switching a near-field's character from a potential energy well to a potential energy ridge for negative secondary ions.

Moreover, it is highly desirable that the charge flux balance point creates a slight near-field ridge for the ions of the extracted (desired) polarity. The near-field ridge prevents these ions from being reflected back onto the sample (lost), and insures that the lowest energy ions (e.g. molecular ions) are not selectively removed to the point they are not detectable. Positive offset potentials appear to be more stable than negative offset potentials in our SIMS systems, because the relatively higher emission of negative secondary charged particles promotes better positive offset potential control. Most of the insulating samples in our experience have initially positive offset potentials (an advantage for detecting positive ions). Varying the primary beam kinetic energy and the use of adjustable magnetic fields with these types of insulating samples offers a direct approach for creating a stable near-field ridge for improved detection of negative secondary ions and secondary electrons.

Insights from this investigation have also expanded our perceptions of sample charging issues. In the past, a sample with significant initial temporal shifts in spectral intensities was thought to have some undetermined charging issue. It is now apparent that sample contaminants probably play a significant role in determining the emission ratios of secondary charge and therefore offset potentials. The removal of these contaminants from the surface whether by evaporation in the vacuum or via primary beam sputtering acts to shift the secondary charge emission ratios. When secondary charge emission ratios change, ridge and well near-fields change too. The resulting temporal shifts in ion spectral intensities may be mistakenly interpreted as beam induced sample damage or simple sample charging. In other words, our repertoire of excuses for sample charging has been greatly expanded. However, sample charging is not viewed to be quite as mysterious as it once was.

Self-charge-stabilization mechanisms probably play a significant role in the outcomes of a broad range of instrumental methods. Whether these mechanisms help or hinder is dependent on their successful recognition and exploitation. Analysis of insulators via Auger electron spectroscopy serves as an example. The self-charge-stabilization model for Auger electron spectroscopy mimics the first example discussed in this paper (electron primary beam with secondary electron emission). It is widely recognized that the secondary electron yield must be greater than one ($\gamma > 1$) to avoid serious sample charging problems. Some of the methods commonly used to accomplish this include: Varying the primary beam's kinetic energy (varying the yield), varying the tilt angle of the specimen (varying the yield), and using low energy auxiliary primary beams of positive ions or electrons (varying the effective yield) [14]. When these strategies are successful, self-charge-stabilization mechanisms act to limit sample charging. However, more optimal electrode geometry provides the opportunity for tighter sample potential control (e.g. leakage rings or equivalent). Gains in these areas could significantly reduce the magnitude of sample charging as well as facilitate improved instrument stability and ease-of-use when analyzing insulators via Auger electron spectroscopy.

In conclusion, self-charge-stabilization mechanisms appear to provide an effective means for understanding and controlling sample charging where applicable. Self-charge-stabilization mechanisms probably influence the behavior of many instrumental methods and experiments whether they are recognized or not. Hopefully the concepts presented in this paper will lead to more recognition and exploitation of the opportunities that self-charge-stabilization methods appear to afford.

Acknowledgements

This research was supported by the US Department of Energy, Office of Biological and Environmental Research under contract DE-AC07-94ID13223.

References

[1] N.M. Reed, J.C. Vickerman, in Practical Surface Analysis: Ion and Neutral Spectroscopy, 2nd ed., D. Briggs, M.P. Seah (Eds.), Wiley, New York, 1992, Vol. 2, pp. 307–312.
[2] D. Briggs, A.B. Wootton, Surf. Interface Anal. 4 (1982) 109.
[3] A.D. Appelhans, D.A. Dahl, J.E. Delmore, Anal. Chem. 62 (1990) 1679.
[4] D. Briggs, M.J. Hearn, Int. J. Mass Spectrom. Ion Processes 67 (1985) 47.
[5] David A. Dahl, SIMION 3D Version 6.0 User's Manual, INEL-95/0403 (1995).
[6] A. Benninghoven, R.G. Rudenauer, H.W. Werner, in Secondary Ion Mass Spectrometry Basic Concepts, Instrumental Aspects, Applications and Trends, Wiley, New York, 1987, p. 756.
[7] A. Benninghoven, R.G. Rudenauer, H.W. Werner, in Secondary Ion Mass Spectrometry Basic Concepts, Instrumental Aspects, Applications and Trends, Wiley, New York, 1987, p. 165.
[8] J.E. Delmore, A.D. Appelhans, E.S. Peterson, Int. J. Mass Spectrom. Ion Processes 146/147 (1995) 15.
[9] J.C. Ingram, G.S. Groenewold, A.D. Appelhans, J.E. Delmore, J.E. Olson, D.L. Miller, Environ. Science Tech. 31 (1997) 402.
[10] G.S. Groenewold, J.C. Ingram, J.E. Delmore, A.D. Appelhans, J. Am. Soc. Mass Spectrom. 6 (1995) 165.
[11] A.D. Appelhans, G.S. Groenewold, J.C. Ingram, J.E. Delmore, D.A. Dahl, in Proceedings of the 10th International Conference on Secondary Ion Mass Spectrometry, SIMS X,

Oct. 1–6, 1994, Muenster, Germany, Wiley, New York, 1997, pp. 935–938.
[12] A.D. Appelhans, J.C. Ingram, G.S. Groenewold, D.A. Dahl, J.E. Olson, J.E. Delmore, in Proceedings of the 7th European Conference on Applications of Surface Analysis, Goteborg, Sweden, June 16–20, 1997, Wiley, New York, 1997, pp. 549–552.
[13] P. Humphrey, A.J. Eccles, P. Mann, J.C. Vickerman, in Proceedings of the 8th International Conference on Secondary Ion Mass Spectrometry, SIMS VIII, Sept. 15–20, Amsterdam, The Netherlands, Wiley, New York, 1991, p. 247.
[14] S. Ichimura, H.E. Bauer, H. Seiler, S. Hofmann, Surf. Interface Anal. 14 (1989) 250.